Energetic proton acceleration and bunch generation by ultraintense laser pulses on the surface of thin plasma targets

T. Okada,[1] A. A. Andreev,[2] Y. Mikado,[1] and K. Okubo[1]
[1]*Faculty of Technology, Tokyo University of Agriculture and Technology, Koganei-shi, Tokyo 184-8588, Japan*
[2]*Institute for Laser Physics, St. Petersburg 199034, Russia*
(Received 4 October 2005; published 4 August 2006)

Energetic proton acceleration from concave targets, the front of which were irradiated with 40 fs laser pulses with an intensity of 10^{20} W/cm^2, has been studied as a function of the depth of the concave shape. Three kinds of targets, a triangular concave target, a circular concave target and a parabolic concave target are considered. When the depth of the concave shape was varied, the peak proton energy showed a maximum. The underlying mechanism for the existence of a maximum peak proton energy is presented by tracing the proton trajectory. It is concluded that a parabolic concave target is the best, among the targets considered, for accelerating a proton beam, since a proton beam from a parabolic concave target goes through the strongest electric field.

DOI: 10.1103/PhysRevE.74.026401 PACS number(s): 52.38.Kd, 52.50.Jm, 52.65.Rr

I. INTRODUCTION

This paper reports the investigation of the influence of the depth of the concave shape on energetic proton acceleration by ultraintense laser interaction.

II. HIGH-ENERGY ELECTRON GENERATION AND ENERGETIC PROTON ACCELERATION

We consider various types of targets to analyze the mechanism of proton acceleration in plasma layers with smooth density gradients. Based on the developed model and 2D particle-in-cell (PIC) simulations, the optimal foil target shape needed to produce maximal accelerated proton beam is investigated [1,2,4–9]. Calculations of proton mobility were carried out for a plasma with the initial density profile shown in Fig. 1. Simulations were performed for a laser wavelength λ of 1.06 μm, beam spot radius R of 1.5λ, laser intensity I of 10^{20} W/cm^2 and pulse duration τ of 40 fs. The laser pulse is linearly polarized, normally incident, and the intensity distribution has a Gaussian shape in space. The maximum electron density is $n_e=4n_c$, where n_c is the critical density. The simulation region and number of particles were $118\lambda\times17\lambda$ and 2.5×10^6, respectively.

Proton acceleration depends critically on the efficiency of the transfer of laser energy into high-energy electrons, since these electrons are the source of the required strong electrostatic field. Numerical simulations show that in the case of a short (40 fs) laser pulse with an intensity I of around 10^{19} W/cm^2, the absorption coefficient is independent of the angle of incidence, with the absorption being about 14% in the absence of a prepulse. Similar absorption coefficient values and a plasma density gradient length L dependence of the absorption coefficient are reported in Ref. [10] for a 130 fs pulse with an intensity of 4×10^{19} W μm^2/cm^2. According to our simulations [11–13], as the laser intensity is raised to 10^{20} W/cm^2, the absorption coefficient increases up to 30%, which demonstrates the influence of proton movement on absorption at high intensities even for a very short pulse. The analytical scaling [14,15] of the average electron absorption coefficient $\eta(\delta g, I)$ is close to the PIC simulation data,

$$\eta(\delta g, I) = 0.05 + (0.1 + 0.01\,\delta g) I_{18}/(15 + I_{18})^{0.8}. \quad (1)$$

Here, I_{18} is the laser intensity in units of 10^{18} W/cm^2, $\delta g = L\omega/c$ where L is the density gradient length, ω is the laser frequency and c is the velocity of light.

In Fig. 2, the simulation results of the electron absorption coefficient with the plasma gradient are plotted with open circles for a slab plasma target. The solid line is the analytical prediction [Eq. (1)] and the dotted line is the numerical fit to the simulation results for $I=10^{20}$ W/cm^2.

The absorbed laser energy is transferred to high-energy electrons, which are ejected from the rear foil surface. These electrons produce an ambipolar field that causes a proton beam to be emitted from the rear foil surface. We consider the direction of a proton beam from the rear foil surface. The average energy of the high-energy electrons ε_{eh} is then calculated from the ponderomotive potential for linear polarized laser radiation [3,16] as

$$\varepsilon_{eh} = m_e c^2 (\sqrt{1 + I_{18}\lambda_\mu^2/2.74} - 1) \quad (2)$$

where m_e is the electron mass and λ_μ is in microns (μm). The maximal proton energy can be estimated from the following formula [17,18]:

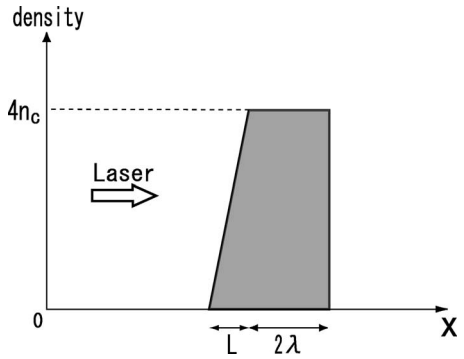

FIG. 1. Target density profile.

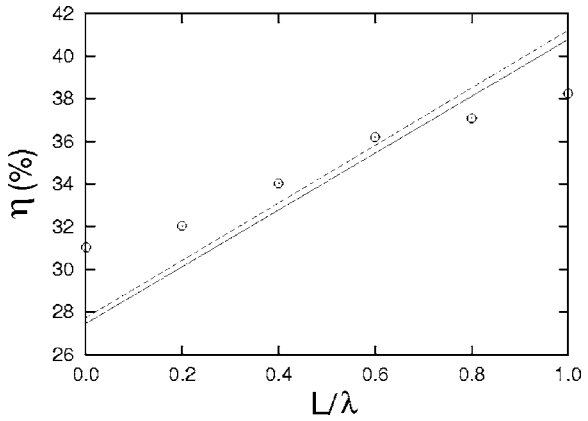

FIG. 2. The electron absorption coefficient vs plasma gradient length. Open circles represent the simulation results for $I=10^{20}$ W/cm^2. Analytical prediction obtained using Eq. (1) for $I=10^{20}$ W/cm^2 is shown by the solid line and the numerical fit to the simulation results (open circles) by the dotted line.

$$\varepsilon_i = 2\varepsilon_{eh}\{\ln[\omega_{pi}t_{ef}/\sqrt{2e_E} + \sqrt{1+(\omega_{pi}t_{ef}/\sqrt{2e_E})^2}]\}^2, \quad (3)$$

where $\omega_{pi}=\sqrt{4\pi n_e e^2/m_i}$, m_i is the proton mass, e is the electron charge, $t_{ef}\approx\tau$ and $e_E=2.718$, etc.

The vector potential dependence of the laser beam intensity on the transverse coordinate y is assumed, as is an exponential drop in skin layer l_s inside the plasma,

$$A_L(x,y) = A_0 \exp(-x/l_s - y^2/2R^2). \quad (4)$$

If the laser intensity is flat in time, the full width at half-maximum (FWHM) of the Gaussian shape is $2R$. The maximum distance h from the foil that the electrons can travel is easily estimated by equating the electrostatic energy of the electrons to the total energy of the electrons yielding [19]

$$h \approx (\varepsilon_{eh}/4\pi n_{eh}e^2)^{1/2}, \quad (5)$$

where $n_{eh}\approx\eta I\tau/\lambda_D$ and λ_D is the Debye radius. At distances larger than h, the electron bunch will expand radially, forming an electron cloud that continues to expand isotropically. Hence, h can be regarded as the critical distance from the surface beyond which the electron cloud can no longer be referred to as an electron beam.

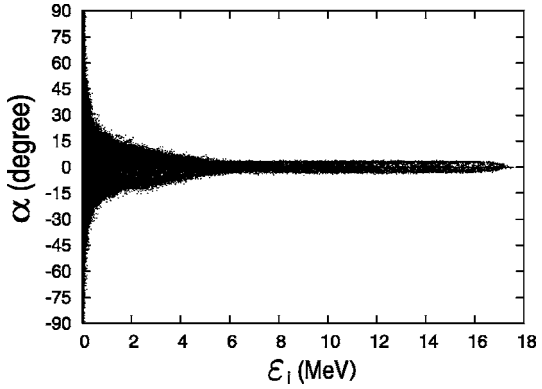

FIG. 3. The angle $\alpha=\sin^{-1}(v_{iy}/v_i)$ of proton motion vs the proton energy ε_i at $\omega t=350$.

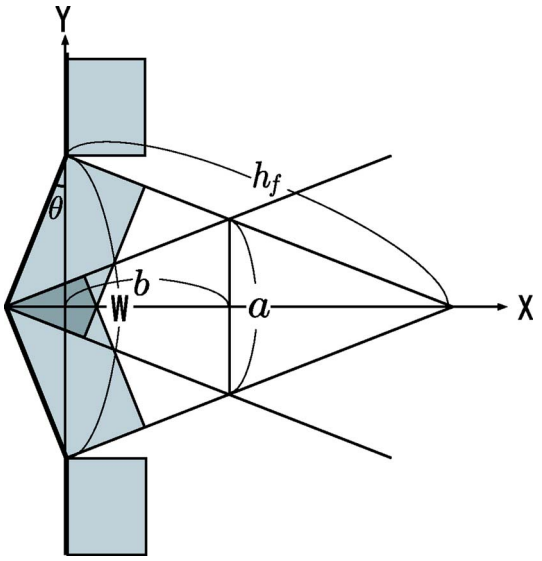

FIG. 4. (Color online) The geometrical structure of the proton fronts crossing from both sides of the target cavity showing the proton jet formation.

The angle of proton divergence at the foil rear, which is determined by the electron cloud and can be estimated from the following formula:

$$\phi_i = \frac{v_{iy}}{v_i} \approx \frac{n_{eh}e^2hR}{\varepsilon_i} \approx \frac{m_e c^2}{\varepsilon_i}\frac{R}{\lambda}\sqrt{\frac{n_{eh}}{n_c}\frac{\varepsilon_{eh}}{m_e c^2}}. \quad (6)$$

Here, the effect of the magnetic field is neglected compared to the electric field. In Fig. 3, the angle α of proton motion vs the proton energy ε_i at $\omega t=350$ ($t=197$ fs) is shown for the slab target. Equation (6) gives the angle $\alpha=\sin^{-1}\phi_i\approx 4°$ [at $\varepsilon_{eh}\approx 2.8$ MeV, $\varepsilon_i\approx 7.5$ MeV from Eqs. (2) and (3), $n_{eh}=0.1n_c$ and $R=1.5\lambda$], which agrees well with the simulation result $|\alpha|\leqslant 5°$ in Fig. 3.

We can thus conclude that under the conditions used here, proton ejection is almost normal to the target surface. Therefore, convergence of the proton beam can be achieved by rearranging the foil target into a curve $y=y(x)$. From Ref.

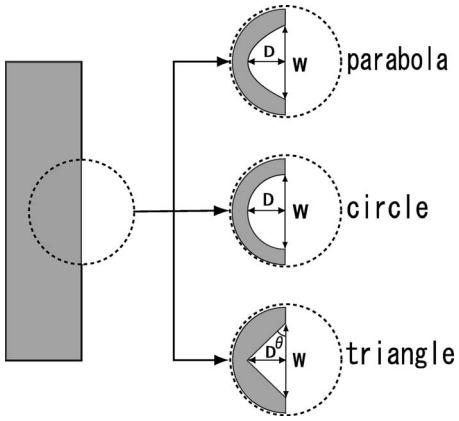

FIG. 5. The geometry of the target containing the concave cavity.

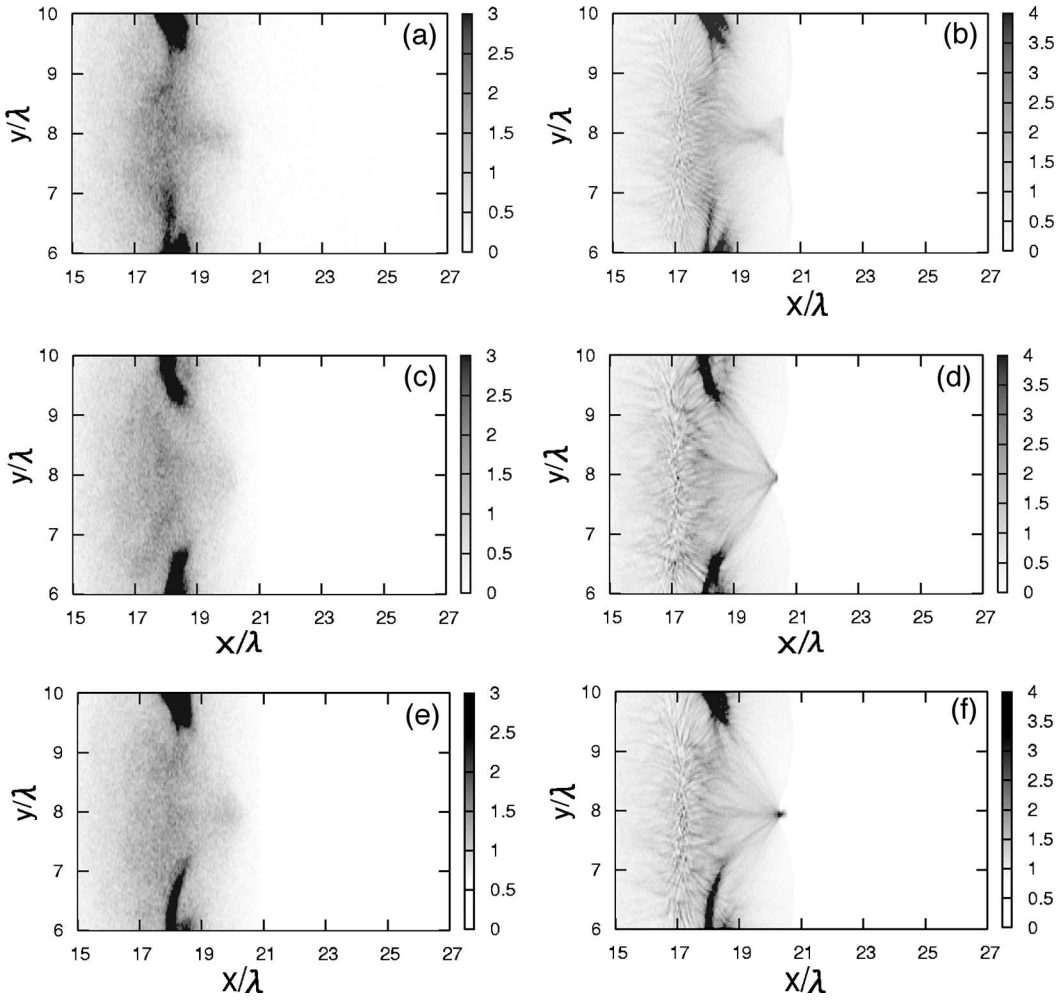

FIG. 6. Spatial distribution of (a) electron density and (b) proton density from a triangular concave target with $D=\lambda$ at $\omega t=350$. Spatial distribution of (c) electron density and (d) proton density from a circular concave target with $D=\lambda$ at $\omega t=350$. Spatial distribution of (e) electron density and (f) proton density from a parabolic concave target with $D=\lambda$ at $\omega t=350$.

[15], the proton trajectory of the particle initially located at the boundary point $x_0, y(x_0)$ of the surface is

$$x(y) = x_0 + \int_y^{y(x_0)} \frac{dy}{\sqrt{y'^2(x_0) - 4\beta \ln[y(x_0)/y]}}, \tag{7}$$

where $\beta = J + c_s^2/v_i^2$, $J = ZeJ_i(1-K)/(m_i v_i^3)$, c_s is the proton sound velocity, v_i is the proton velocity, Z is the charge number of proton, J_i is the total electric current of the proton beam and $K = n_{eh}/n_e$. The angle of proton movement to vacuum from the surface $y=y(x)$ at the initial coordinate $[x_0, y(x_0)]$ is determined by the perpendicular to this surface,

$$\left.\frac{dy}{dx}\right|_{x=x_0} = -\frac{1}{y'(x_0)}. \tag{8}$$

Without interaction in the proton bunch, the proton trajectory is a straight line: $y(x) = y(x_0) - (x - x_0)/y'(x_0)$. The distance from the foil at which the beam is focused depends on the foil profile and laser beam parameters. The minimum radius of the focused beam is achieved when the expression under the square root in Eq. (7) is zero,

$$y_{\min}(x_0) = y(x_0)\exp\left(-\frac{y'^2(x_0)}{4\beta}\right). \tag{9}$$

If $y(x_0) - y_{\min}(x_0) \ll y(x_0)$, then instead of the exact trajectory described by Eq. (7) it is convenient to use the Tailor expansion,

$$y(x) = y(x_0) - \frac{(x - x_0)}{y'(x_0)} - \frac{\beta(x - x_0)^2}{y(x_0)}. \tag{10}$$

Here, the parameter x_0 changes while coexisting with the shape of the surface $y(x_0)$. The envelope can be found by the same method but more complicated for the family of exact trajectories from Eq. (7).

In Fig. 4, the proton focusing effect was verified at first using a model in which protons are ejected from a cone-shaped cutout of angle θ on the rear surface of the foil target. A needle-shaped jet of protons is then created along the central axis of the cutout. The formation of the area of increased density can be explained by geometrical considerations. The diameter of the focal area a is connected to the diameter of the cavity W through the relationship $a = W/(2\cos^2\theta)$. Dis-

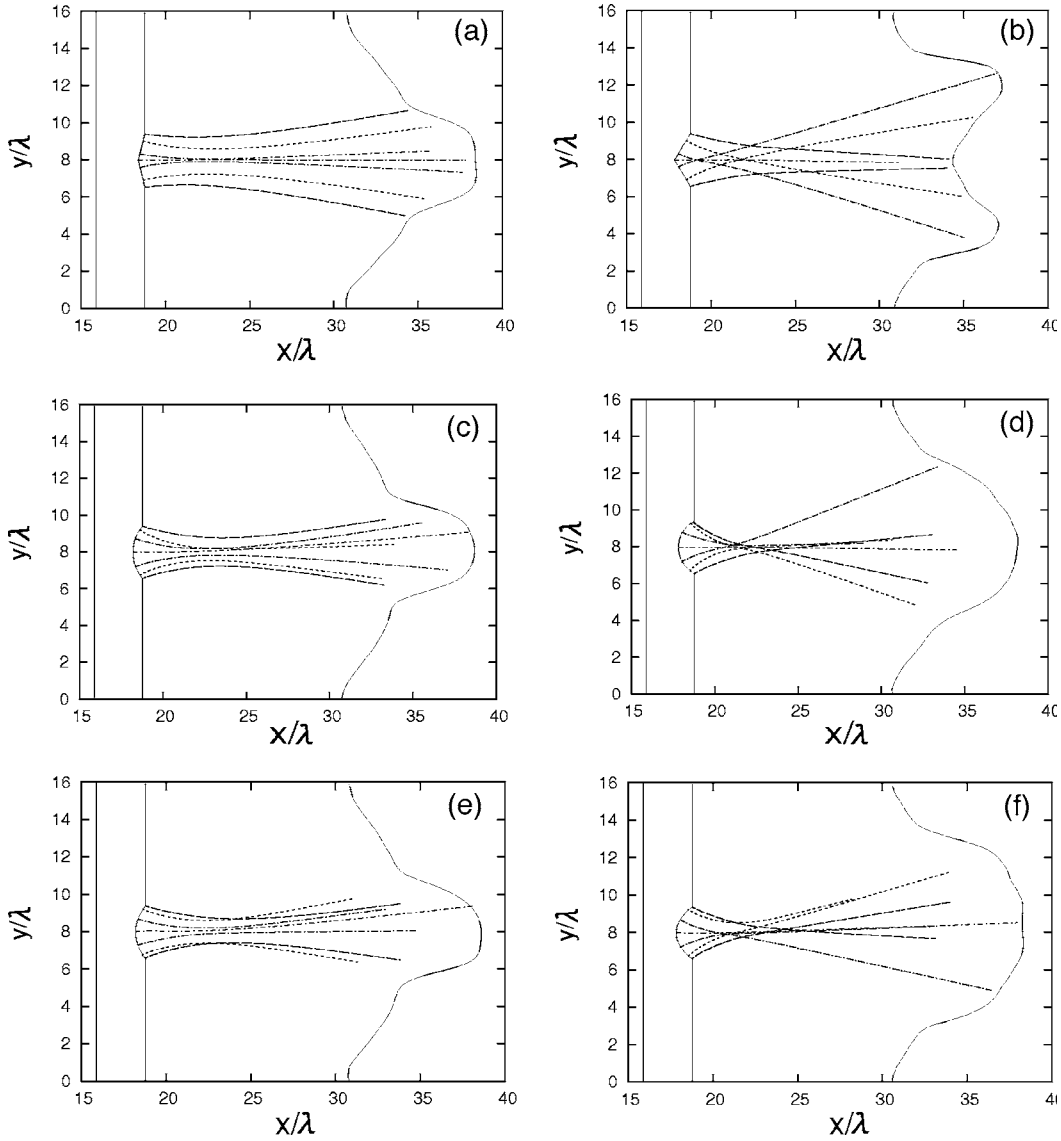

FIG. 7. Proton beam trajectories and contour of (a) $D=0.4\lambda$ and (b) $D=\lambda$ from a triangular concave target at $\omega t=800$. Proton beam trajectories and contour of (c) $D=0.6\lambda$ and (d) $D=\lambda$ from a circular concave target at $\omega t=800$. Proton beam trajectories and contour of (e) $D=0.6\lambda$ and (f) $D=\lambda$ from a parabolic concave target at $\omega t=800$.

tances from the surface of the foil to the focal plane and to the focal point are $b=a/(2|\tan 2\theta|)$ and $h_f=W/(2\sin\theta)$, respectively. In real experiments, the target would be located at this distance for irradiation with protons. Note that in our simulations the trajectories of the separated protons are practically rectilinear. Comparing the position of the geometrical focal point with the calculated focal point yields an estimate for K, which is the degree of charge compensation in the proton beam.

Next we analyzed the proton focusing effect by two other surfaces $y=f_{1,2}(x)$ such as part of a circle and a parabola, respectively,

$$f_1(x)=\sqrt{\left(\frac{(W/2)^2+D^2}{2D}\right)^2-\left(x-\frac{(W/2)^2-D^2}{2D}\right)^2},$$

$$f_2(x)=\frac{W}{2}\sqrt{1+\frac{x}{D}}. \tag{11}$$

Here $W/2$ is the radius of the concave cavity and D is its depth. At $D=W/6$ and $x=-W/12$ the minimal distance from the envelop of the trajectory to the beam axis was calculated from Eq. (11) as $0.36W$ for the circle and $0.35W$ for the parabola. Thus, the parabolic surface is more effective for proton beam focusing because of shorter minimal distance for the parabola than that for the circle. At the Debye radius of fast electrons close to $W/2$ these electrons will concentrate at the center of the cavity. Its electric charge will deviate the direction of the electrostatic field from the normal and increases the electric field at the concave center compared to a plane surface. As a result, the maximal energy of fast protons and focusing will increase. The dependence of the am-

plifying field on the concave angle has a maximum at some point of its value. Thus, not only beam focusing but also the maximal proton energy can be optimized with the use of a tuned (here parabolic) concave shape.

III. ENERGETIC PROTON BUNCH SIMULATION WITH CONCAVE TARGETS

Proton focusing effects were verified using a model in which protons are ejected from concave targets, as shown in Fig. 5. In this simulation, we assume that the length W of the concave target is constant at 3λ, the density gradient length L is constant at λ and the depth D of the concave target is changed from 0 to λ. In Fig. 6, spatial distributions of electron and proton densities at $\omega t=350$ ($t=197$ fs) are shown for the triangular concave target, the circular concave target and the parabolic concave target with $D=\lambda$, respectively. From these figures, bunches of protons can be focused at a given point in space by the curvature of the rear surface of the foil.

In Fig. 7, proton beam trajectories and contours at $\omega t=800$ ($t=449$ fs) are shown for the triangular concave target, the circular concave target and the parabolic concave target, respectively. It can be obviously seen from these figures that the proton beam, accelerated by the strong electric field induced by the region of heightened electron density, is collected near the x-axis direction when y/λ is around 6–10. For the triangular concave target, as in Fig. 7(a), the peak proton energy is increased by changing D from 0 to 0.4λ because the proton beams go through the stronger electric field. However, after $D=0.4\lambda$ the peak proton energy decreased because the proton beams cross the stronger electric field, as seen in Fig. 7(b). For the circular and parabolic concave targets, the acceleration mechanism of the proton beam is the same as for the triangular concave target.

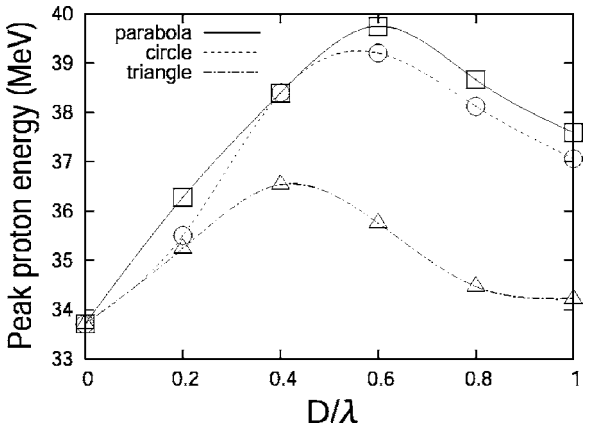

FIG. 8. Peak proton energy vs depth of the concave shape (D/λ) from the triangular, circular, and parabolic concave targets at $\omega t=800$.

IV. CONCLUSIONS

There is a maximum for the peak proton energy as shown in Fig. 8. For the triangular concave target, the peak proton energy is maximum at $D=0.4\lambda$ which corresponds to $\theta\approx 15°$. For the circular concave target, the peak proton energy is maximum at $D=0.6\lambda$ which corresponds to the radius of the circle $r\approx 2.2\lambda$. For the parabolic concave target, the peak proton energy is maximum at $D=0.6\lambda$ which corresponds to $a\approx 0.27$ for the formula of the parabola of $x=a(y-8\lambda)^2/\lambda+18\lambda$. These results show that the parabolic concave target is the best for accelerating a proton beam among the three targets examined in this study.

ACKNOWLEDGMENT

This work was performed under the collaboration program of the Institute of Laser Engineering, Osaka University.

[1] S. C. Wilks, Phys. Fluids B **5**, 2603 (1993).
[2] Y. Sentoku *et al.*, Phys. Rev. E **62**, 7271 (2000).
[3] S. C. Wilks *et al.*, Phys. Plasmas **8**, 542 (2001).
[4] A. Pukhov, Phys. Rev. Lett. **86**, 3562 (2001).
[5] A. P. Fews, P. A. Norreys, F. N. Beg, A. R. Bell, A. E. Dangor, C. N. Danson, P. Lee, and S. J. Rose, Phys. Rev. Lett. **73**, 1801 (1994).
[6] A. Maksimchuk, S. Gu, K. Flippo, D. Umstadter, and V. Y. Buchenkov, Phys. Rev. Lett. **84**, 4108 (2000).
[7] R. A. Snavely *et al.*, Phys. Rev. Lett. **85**, 2945 (2000).
[8] J. Fuchs *et al.*, Nat. Phys. **2**, 48 (2006).
[9] S. P. Hatchett *et al.*, Phys. Plasmas **7**, 2076 (2000).
[10] E. Lefebvre and G. Bonnaud, Phys. Rev. E **55**, 1011 (1997).
[11] A. A. Andreev, K. Yu. Platonov, T. Okada, and S. Toraya, Phys. Plasmas **10**, 220 (2003).
[12] T. Okada, Y. Mikado, T. Kitada, M. Sugie, and A. A. Andreev, Jpn. J. Appl. Phys., Part 1 **44**, 1431 (2005).
[13] A. J. Mackinnon, Y. Sentoku, P. K. Patel, D. W. Price, S. Hatchett, M. H. Key, C. Andersen, R. Snavely, and R. R. Freeman, Phys. Rev. Lett. **88**, 215006 (2002).
[14] A. A. Andreev and K. Yu. Platonov, Laser Part. Beams **18**, 81 (2000).
[15] A. A. Andreev, T. Okada, K. Yu. Platonov, and S. Toraya, Laser Part. Beams **22**, 431 (2004).
[16] S. Okihara *et al.*, J. Nucl. Sci. Technol. **39**, 1 (2002).
[17] P. Mora, Phys. Rev. Lett. **90**, 185002 (2003).
[18] M. Kaluza, J. Schreiber, M. I. K. Santala, G. D. Tsakiris, K. Eidmann, J. Meyer-ter-Vehn, and K. J. Witte, Phys. Rev. Lett. **93**, 045003 (2004); Y. Oishi *et al.*, Phys. Plasmas **12**, 073102 (2005).
[19] V. T. Tikhonchuk, Phys. Plasmas **9**, 1416 (2002); A. A. Andreev, A. G. Zhidkov, A. Sasaki, and K. Yu. Platonov, Plasma Phys. Controlled Fusion **44**, 1243 (2002).